Centrifugal stretching along the ground state band of ^{168}Hf

A. Costin,[1,2,3] M. Reese,[3] H. Ai,[4] R. F. Casten,[4] K. Dusling,[1] C. R. Fitzpatrick,[4,5] G. Gürdal,[4,6] A. Heinz,[4] E. A. McCutchan,[4] D. A. Meyer,[4] O. Möller,[3] P. Petkov,[2,7] N. Pietralla,[1,2,3] J. Qian,[4] G. Rainovski,[1,8] and V. Werner[4]

[1]*Nuclear Structure Laboratory, SUNY at Stony Brook, Stony Brook, New York 11794-3800, USA*

[2]*Institut für Kernphysik, Universität zu Köln, D-50937 Köln, Germany*

[3]*Institut für Kernphysik, Technische Universität Darmstadt, D-64289 Darmstadt, Germany*

[4]*A. W. Wright Nuclear Structure Laboratory, Yale University, New Haven, Connecticut 06520, USA*

[5]*University of Surrey, Guildford, Surrey GU2 7XH, United Kingdom*

[6]*Clark University, Worcester, Massachusetts 01610, USA*

[7]*INRNE, Bulgarian Academy of Sciences, 1784 Sofia, Bulgaria*

[8]*Faculty of Physics, St. Kliment Ohridski University of Sofia, 1164 Sofia, Bulgaria*

(Received 10 July 2008; published 10 February 2009)

The lifetimes of the $J^\pi = 4^+, 6^+, 8^+$, and 10^+ levels along the ground state band in ^{168}Hf were measured by means of the recoil distance Doppler shift (RDDS) method using the New Yale Plunger Device (NYPD) and the SPEEDY detection array at Wright Nuclear Structure Laboratory of Yale University. Excited states in ^{168}Hf were populated using the ^{124}Sn(^{48}Ti,4n) fusion evaporation reaction. The new lifetime values are sufficiently precise to clearly prove the increase of quadrupole deformation as a function of angular momentum in the deformed nucleus ^{168}Hf. The data agree with the predictions from the geometrical confined β-soft (CBS) rotor model that involves centrifugal stretching in a soft potential.

DOI: 10.1103/PhysRevC.79.024307 PACS number(s): 21.10.Tg, 25.70.Gh, 27.70.+q

I. INTRODUCTION

Geometrical concepts in terms of rotational and vibrational structures have been used to classify nuclear data for more than half a century. Understanding the mechanisms that determine whether a given nuclear system belongs to a given class is a fundamental goal of nuclear structure physics. In particular, shape transitions between distinct classes are of outstanding interest. Recently, a simple and successful description for the nuclear structure near the spherical-to-axially deformed shape phase transitional points was suggested by Iachello in terms of the X(5) model [1]. Indeed, evidence for nuclei displaying shape phase transitional properties was reported [2–4]. Iachello's analytical approximation to the geometrical Bohr Hamiltonian [5] uses an infinite square well potential that allows for large fluctuations in the quadrupole deformation parameter β. An important prediction of the model is an increase of the transitional quadrupole moments along the ground state band as a function of angular momentum. This phenomenon of centrifugal stretching is clearly observable in the $E2$ data of transitional nuclei close to the critical point, such as ^{150}Nd [3], ^{152}Sm [2], and ^{154}Gd [4], that are characterized by a soft potential in β with low stiffness and consequently by an $R_{4/2} = E_x(4_1^+)/E_x(2_1^+)$ value of about 2.9. Their transitional quadrupole moments in the ground state band increase by about 10% from the 2_1^+ state to the 10_1^+ state. These observations have been made in a model independent way from high-precision lifetime measurements performed with the recoil distance Doppler shift (RDDS) method [6]. This technique allows for the measurements of transitional quadrupole moments with an experimental uncertainty of about 2% using the differential decay curve method [7,8].

The X(5) approximation has been generalized to a simple, one-parameter analytical model for the quadrupole-collective structures of transitional nuclei in terms of the confined β-soft (CBS) rotor model [9]. The CBS rotor model describes axially symmetric nuclei with structural observables $R_{4/2} = 2.90$ to 3.33, i.e., from the shape phase transitional point to the rigid rotor limit. The CBS rotor model has been shown to predict successfully the properties of the β excitation [9] and to describe the energies in the ground state bands of strongly deformed nuclei with an accuracy of 1/1000 [10], one to two orders of magnitude more precisely than the rigid rotor. There have been other successful models in describing the deviations from the rigid rotor, as for example the Variable Moment of Inertia (VMI) model [11], which parametrizes a change in the nuclear moment of inertia $\mathcal{I}$ in a semiclassical way with a softness parameter σ. Note that within the VMI description, the variation of $\mathcal{I}$ with angular momentum J is independent of a particular mechanism (e.g., centrifugal stretching, decrease in pairing energy with angular momentum). On the contrary, in the framework of the CBS model, the deviations from the rigid rotor limit are modeled in terms of centrifugal stretching of the spinning deformed nucleus with increasing angular momentum in a soft potential of the nucleus in terms of the quadrupole deformation parameter β. According to this and other geometrical models, the phenomenon of centrifugal stretching is universal and not limited to a few transitional nuclei near the shape phase transitional point. However, the effects expected by the modern geometrical models are quite small. The average deformation is expected to increase by a fraction between 0 and about 10% from the ground state to the 10_1^+ state depending on the stiffness of the nucleus with respect to the quadrupole deformation parameter β. Because of the limit of precision for lifetime measurements, observation of the predicted small centrifugal stretching of more rigidly deformed nuclei with $R_{4/2}$ values of about 3.3 is still not

possible because the effect to be measured is predicted by the CBS rotor model to be of the same size as or even smaller than the typical experimental uncertainties of modern lifetime methods. To push the observations of centrifugal stretching toward the region of more rigidly deformed nuclei it would be interesting to extend the precision lifetime information to nuclei with stiffness greater than that of those near the critical point. Among nuclei in the rare earth region, ^{168}Hf has an $R_{4/2}$ ratio of 3.11, which is intermediate between the value of 2.90 predicted by the X(5) solution close to the critical point of the shape phase transition and the value of 3.33 for the rigid rotor limit. ^{168}Hf seems to be a suitable candidate for observing centrifugal stretching in a more rigidly deformed nucleus in the $A \approx 170$ mass region. The CBS rotor model predicts centrifugal stretching, i.e., an increase of the transitional quadrupole moment with increasing angular momentum, of about 8% from the 2_1^+ state to the 10_1^+ state for this nucleus. Precise enough and reliable lifetime information is not available for it. Lifetime measurements on the ground band of ^{168}Hf were previously done [12] with the RDDS method in singles mode. This method is known to suffer from systematic uncertainties due to unobserved feeding and contaminants. Making a precision lifetime measurement for ^{168}Hf would allow for a precision test of the CBS rotor model and could be decisive on the long standing question of the universal existence of centrifugal stretching in strongly deformed rare earth nuclei. Relative transition rates between low-spin states of ^{168}Hf have recently been studied by some of us [13]. The relevant modern geometrical models all agree on the amount of centrifugal stretching in the ground state band of ^{168}Hf.

II. EXPERIMENT AND ANALYSIS

The purpose of the experiment was to measure lifetimes τ along the ground state band in ^{168}Hf with uncertainties of about 5–10%. This accuracy would result in data on transitional quadrupole moments with uncertainties of about 2–3% that would yield sufficient sensitivity to the predicted centrifugal stretching. Medium spin yrast states of ^{168}Hf were populated using the ^{124}Sn(^{48}Ti,4$n\gamma$)^{168}Hf fusion evaporation reaction at the Tandem facility of Wright Nuclear Structure Laboratory (WNSL) of Yale University. Figure 1 shows a part of the level scheme of ^{168}Hf that is relevant for this article. A 190 MeV ^{48}Ti beam bombarded a 1 mg/cm^2 thick ^{124}Sn self-supporting target. Recoiling nuclei were stopped in a 10 mg/cm^2 ^{197}Au stopper. The target and stopper foils were mounted parallel in the New Yale Plunger Device (NYPD). The SPEEDY array was used for γ-ray detection. It consisted of nine Compton-suppressed segmented CLOVER Ge detectors positioned in three groups (rings), where each ring contains only detectors that are positioned at the same angle with respect to the direction of the beam: one detector at 0° and four detectors at 41.5° in forward position, and four detectors at 138.5° in backward position. Measurements were performed at 12 different distances between the target and the stopper foils, ranging from 12 to 290 μm, for time intervals between 5 to 11 h, necessary to be able to determine lifetimes in the interval 1 to 50 ps at a $v/c \approx 2\%$ of the recoiling nuclei.

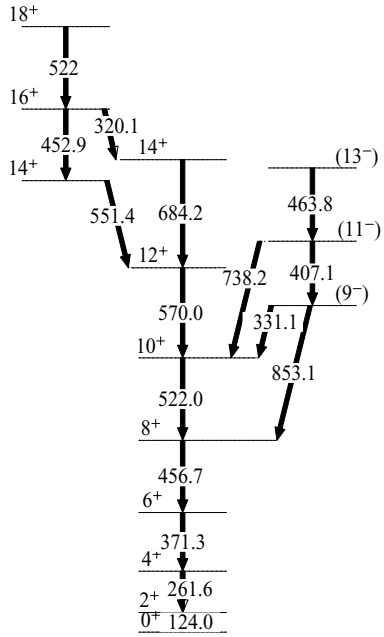

FIG. 1. Partial level scheme of ^{168}Hf relevant to our analysis. New values for the lifetimes of the 4^+, 6^+, 8^+, and 10^+ states were obtained.

Data were recorded with a $\gamma\gamma$ trigger and then sorted into $\gamma\gamma$-coincidence matrices.

The method we used for the analysis of our RDDS data is called the differential decay curve method (DDCM). It was developed by Dewald *et al.* [7,8]. The DDCM applied to measurements in coincidence mode solves problems associated with observed and unobserved feeding and its time behavior. Starting with the time evolution of the population $n_i(t)$ of a level i, it has been shown [7,8] that the lifetime $\tau(x)$ of the level of interest i directly populated by transition B and which depopulates by transition A is

$$\tau_i(x) = \frac{\{B_s, A_u\}(x)}{v\frac{d}{dx}\{B_s, A_s\}(x)}. \tag{1}$$

In this equation, v is the mean velocity of the recoiling nuclei. It is directly obtained from the energy separation between the unshifted γ-ray transition and its corresponding shifted line. The braces denote the Doppler shifted (s) and unshifted (u) coincidence intensities of transition A when a coincidence gate is set on the shifted component of the populating transition B. The equation holds true at each target-to-stopper distance x; therefore one expects to measure a constant lifetime τ throughout. Deviations from a straight line in the sensitive region of a τ vs x plot point to systematic errors in the analysis.

Equation (1) can be generalized for the case when a gate is set on the shifted component of an indirectly feeding transition C, with C in the same cascade as A and B:

$$\tau_i(x) = \frac{\{C_s, A_u\}(x) - \alpha\{C_s, B_u\}(x)}{v\frac{d}{dx}\{C_s, A_s\}(x)}, \tag{2}$$

with

$$\alpha = \frac{\{C_s, A_u\} + \{C_s, A_s\}}{\{C_s, B_u\} + \{C_s, B_s\}}. \tag{3}$$

The uncertainty related to Eq. (2) is greater than that in the case of direct gating so it is employed only in cases when gating on the directly populating transition is not possible due to nearby contaminants.

For each target-to-stopper distance x, eight matrices were sorted corresponding to the possible combinations of the three groups, except for the zero-zero combination, where only one detector is involved. Of the eight matrices only the four corresponding to the 41.5° and 138.5° detectors were used in the analysis. The groups involving the zero degree detector have sensibly less counts than the others, making the determination of peak areas difficult. At a given distance, a lifetime is determined for each group by gating on the shifted component of a direct or indirect feeding transition and measuring the peak areas of the shifted and unshifted depopulating transition or direct populating and depopulating transitions, respectively. Lifetimes corresponding to one group but different distances are averaged, thus presenting a unique lifetime for the group. The distances selected to provide lifetimes are the ones in the region of sensitivity, which is the time interval, or equivalently the distance interval, where the decay curve of a given level depends the most on the lifetime of this level. In practice, these are the distances where the numerator and the denominator of Eq. (1) are not close to zero. A final lifetime is determined by averaging over the lifetimes provided by each group. Figure 2 shows the γ-ray spectra of the $6^+ \rightarrow 4^+$ transition obtained at three different distances by gating on the direct feeding transition.

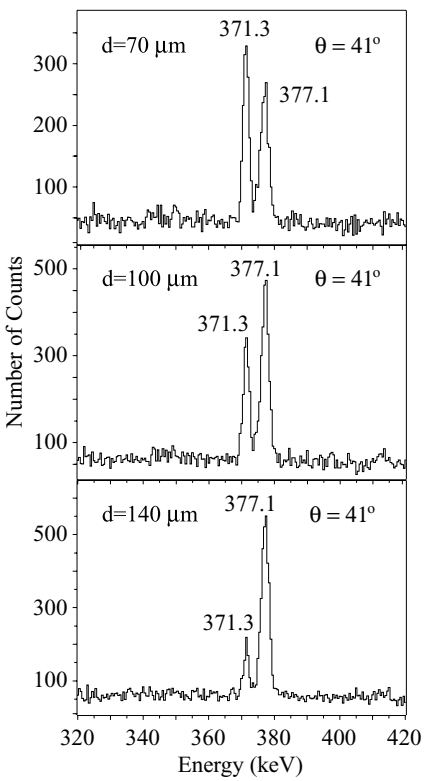

FIG. 2. Unshifted and forward shifted components of the $6_1^+ \rightarrow 4_1^+$ transition in ^{168}Hf at three different distances in gated spectra.

III. RESULTS

The 4^+ state is populated by a 371.3 keV transition and depopulates by a 261.6 keV transition as can be seen in Fig. 1. Gating on the shifted components of the populating transition did not pose any problems so that we could obtain four statistically independent lifetimes corresponding to the four groups that were analyzed. They are as follows: 43.9 ± 0.7 ps for the (41.5°,41.5°) group combination, 44.3 ± 0.6 ps for (138.5°,138.5°), 42.9 ± 0.6 ps for (41.5°,138.5°), and 45.7 ± 0.7 ps for (138.5°,41.5°). As an example, the data and DDCM analysis for the backward-backward combination are shown in Fig. 3. The adopted lifetime of the level is

$$\tau(4_1^+) = 44.2 \pm 2.1 \text{ ps}. \quad (4)$$

The error is the average of two differences: one calculated by subtracting the average lifetime of the four group combinations from the highest lifetime and the other by subtracting the lowest lifetime from the average. Thus it is a maximal error. The corresponding $B(E2; 4_1^+ \rightarrow 2_1^+)$ transition probability is 244 ± 11 W.u.

The 6^+ state is populated by a 456.7 keV transition. Direct gating was possible only in the backward groups because of a contaminant $13^- \rightarrow 11^-$ transition at 463.8 keV that originates from a decay into the ground state band above the 6^+ state and coincides with the forward shifted component of the $8^+ \rightarrow 6^+$ transition. In addition to direct gating on the directly populating transition we also performed indirect gating on the $14^+ \rightarrow 12^+$ transition at 551.4 keV to check the consistency

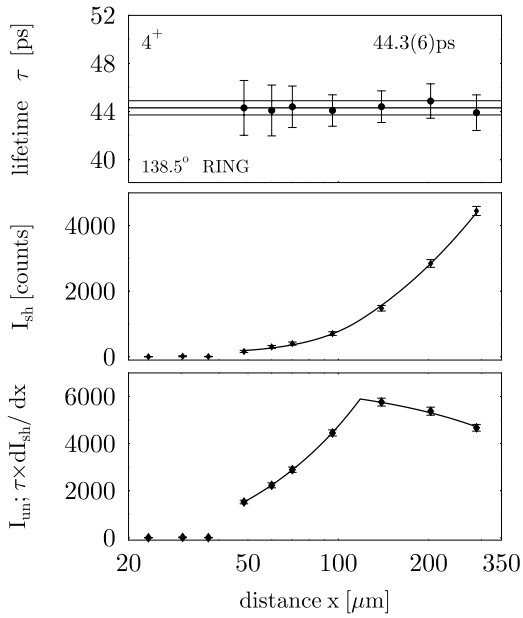

FIG. 3. Lifetime of the 4^+ state determined in the backward ring. The middle panel shows the shifted intensity at different distances. A continuous curve is fitted through the points to calculate the derivative. In the bottom panel, a curve that represents the product between the time derivative of the shifted intensities and the lifetime of the level is compared with the experimental unshifted intensity. Out of this comparison, the lifetimes corresponding to each distance in the region of sensitivity are extracted, as seen in the upper panel.

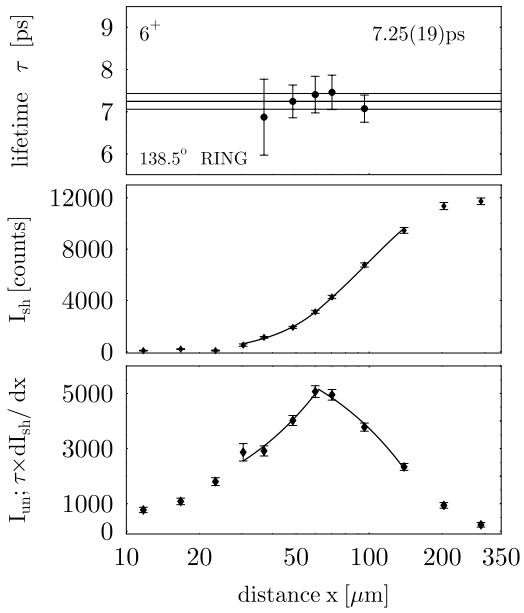

FIG. 4. Lifetime of the 6^+ state determined in the backward ring. See caption of Fig. 3 for further information.

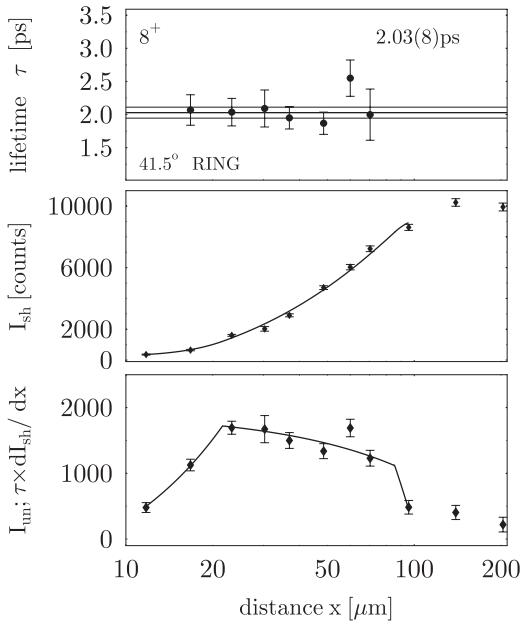

FIG. 5. Lifetime of the 8^+ state determined in the forward ring. See caption of Fig. 3 for further information.

of our results obtained with direct gating. An example is given in Fig. 4 in the case of indirect gating from above. The adopted lifetime obtained is

$$\tau(6_1^+) = 7.1 \pm 0.4 \text{ ps}. \quad (5)$$

We used the same procedure as above for calculating the error. The $B(E2; 6_1^+ \rightarrow 4_1^+) = 283 \pm 17$ W.u.

The 8^+ state is populated by a 522.0 keV transition. It was not possible to gate directly from above because of a $18^+ \rightarrow 16^+$ transition with the same energy located in the ground state band. We gated indirectly from above on the $12^+ \rightarrow 10^+$ transition. This does not immediately solve the problem of the contaminant because when gating indirectly from above one needs to know the intensities of the shifted and unshifted components of the populating and depopulating transitions of the level of interest [see Eqs. (2) and (3)], and the shifted component of the populating transition will still be contaminated by the shifted part of the higher transition. But the unshifted component of the $10^+ \rightarrow 8^+$ transition is not contaminated because of the coincidence requirements we set when gating indirectly from above. We know that all intensity populating the 8^+ level comes from $10^+ \rightarrow 8^+$ 522 keV γ rays and all depopulating intensity is in the $8^+ \rightarrow 6^+$ 456.7 keV γ ray. The total 522 keV intensity (shifted + unshifted), I^t_{522}, that we measure in the cut spectra is the sum of the shifted, $I^s_{10^+\rightarrow 8^+}$, and unshifted, $I^u_{10^+\rightarrow 8^+}$, $10^+ \rightarrow 8^+$ intensity and of the shifted, $I^s_{18^+\rightarrow 16^+}$, $18^+ \rightarrow 16^+$ intensity. Subtracting from I^t_{522} the total 456.7 keV intensity we obtain $I^s_{18^+\rightarrow 16^+}$. Finally, the difference between the shifted 522 keV intensity and $I^s_{18^+\rightarrow 16^+}$ is $I^s_{10^+\rightarrow 8^+}$. Because of the low number of counts when gating indirectly, we summed the cut spectra obtained by gates at forward and backward groups but with the cut spectra in the same group. Thus we obtained two lifetime curves. An example is given in Fig. 5. The adopted lifetime is

$$\tau(8_1^+) = 2.10 \pm 0.26 \text{ ps} \quad (6)$$

and the $B(E2; 8_1^+ \rightarrow 6_1^+) = 348 \pm 43$ W.u.

The 10^+ state is populated by a 570.0 keV transition. In this case we gated directly from above and we followed the exact same steps as for the analysis of the 8^+ lifetime because the problem with the $18^+ \rightarrow 16^+$ contaminant was the same. The resulting lifetime and transition probability are

$$\tau(10_1^+) = 1.02 \pm 0.14 \text{ ps} \quad (7)$$

and

$$B(E2; 10_1^+ \rightarrow 8_1^+) = 368 \pm 52 \text{ W.u.}, \quad (8)$$

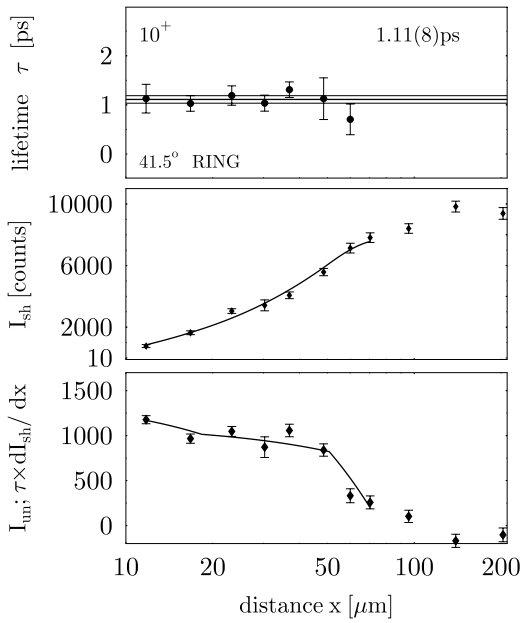

FIG. 6. Lifetime of the 10^+ state determined in the forward ring. See caption of Fig. 3 for further information.

TABLE I. Lifetimes and their corresponding $B(E2)$ transition probabilities along the ground state band in ^{168}Hf. The excitation and transition energies along with the electron conversion coefficients α were taken from Ref. [17].

J ($\hbar$)	$E(J)$ (keV)	$E_\gamma(J \to J-2)$ (keV)	$\tau(J)$ (ps)	$\alpha(J \to J-2)$	$B(E2; J \to J-2)$ (e^2b^2)	
					This work	Bochev *et al.*[a]
2	124.0	124.0(2)		1.57		0.838(35)
4	385.6	261.6(2)	44.2(21)	0.122	1.344(63)	1.152(116)
6	756.9	371.3(2)	7.1(4)	0.043	1.560(92)	1.300(127)
8	1213.6	456.7(3)	2.10(26)	0.0245	1.91(24)	1.398(132)
10	1735.6	522.0(3)	1.02(14)	0.0175	2.03(28)	1.422(216)

[a]Taken from Ref. [12].

respectively. An example with the lifetime measured in the forward group is given in Fig. 6. Because of the Doppler-shift attenuation (DSA) effects in the stopper, the lifetime given above may represent a lower limit of the expected lifetime. These DSA effects appear when the lifetime of the level is comparable to the slowing down time of the recoiling ^{168}Hf nuclei, which amounts to approximately 1.3 ps. For our analysis, this means that some of the intensity we measure in the shifted peaks actually belongs to the unshifted component and the net effect would be a lowering of the deduced lifetime. This systematic effect must be corrected for. The correction amounts to 10–15% as indicated in Refs. [14] and [15] for the 10_1^+ state discussed above and it is not necessary for lifetimes greater than 2 ps, at this stopping time. To more precisely account for this effect, one would need to do a dedicated experiment or to use a DSA analysis method [8] or treat it according to the technique described in Ref. [16], which Refs. [14] and [15] follow. We consider our correction sufficient.

A summary of the experimental results is given in Table I. Previous literature values by Bochev *et al.* [12] are also given. We stress that they were obtained in a RDDS measurement in singles mode. The analysis of such data encounters known problems with systematic errors. For the purposes of the following discussion we use our coincidence data, only.

IV. DISCUSSION

In the rigid rotor model the moments of inertia are fixed, they do not change whether the nucleus is spinning slower or faster as seen in Eq. (9).

$$E_{\mathrm{RR}}(J) = \frac{\hbar^2}{2\mathcal{I}_{\mathrm{RR}}} J(J+1). \tag{9}$$

The change in energy is obtained entirely by increasing or decreasing the angular momentum. In the geometrical CBS rotor model, the level energies in the ground state band are given by the expression

$$E_{\mathrm{CBS}}(J) = \frac{\hbar^2}{2B\beta_{\max}^2}\left[\left(z_{J,1}^{r_\beta}\right)^2 - \left(z_{0,1}^{r_\beta}\right)^2\right], \tag{10}$$

with $z_{J,s}^{r_\beta}$ being the sth zero of the parametric combination

$$D_{J,s}^{r_\beta}(z) = J_{\nu(J)}(z)\, Y_{\nu(J)}(r_\beta z) - J_{\nu(J)}(r_\beta z)\, Y_{\nu(J)}(z) \tag{11}$$

of first order, $J_\nu(z)$, and second order, $Y_\nu(z)$, Bessel functions of the irrational order $\nu(J) = \sqrt{[J(J+1) - K^2]/3 + 9/4}$. The only structural model parameter $r_\beta = \beta_{\min}/\beta_{\max}$ denotes the ratio of the boundaries of the infinite square well potential $V(\beta)$. To interpret the results in terms of variable moments of inertia, we define angular momentum dependent moments of inertia in the spirit of the rotor model by

$$E_{\mathrm{CBS}}(J) = \frac{\hbar^2}{2\mathcal{I}_{\mathrm{CBS}}(J)} J(J+1) \tag{12}$$

and analogously for the experimental energy

$$E_{\mathrm{Expt.}}(J) = \frac{\hbar^2}{2\mathcal{I}_{\mathrm{Expt.}}(J)} J(J+1). \tag{13}$$

First, we compare the moments of inertia from the CBS rotor model to the experimental ones. To become independent of any external scales, all energies were normalized to the excitation energy of the first 2^+ state according to

$$\frac{\mathcal{I}(J_1^+)}{\mathcal{I}(2_1^+)} = \frac{E(2_1^+)}{E(J_1^+)} \frac{J(J+1)}{6}. \tag{14}$$

A plot of the rigid rotor, VMI, CBS, and experimental values $\mathcal{I}(J_1^+)/\mathcal{I}(2_1^+)$ is shown in Fig. 7. The agreement between the predictions of the CBS model and the VMI model

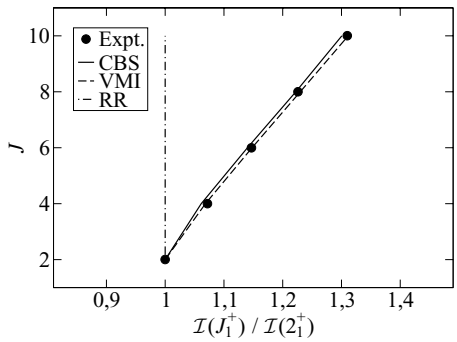

FIG. 7. Theoretical and experimental $\mathcal{I}(J_1^+)/\mathcal{I}(2_1^+)$ ratios as a function of spin, J, in ^{168}Hf. The vertical line represents the rigid rotor while the dashed curve shows the VMI prediction as given in Ref. [11] for the choice of the softness parameter $\sigma = 0.015$. The solid curve represents the CBS rotor model prediction with the model parameter $r_\beta = 0.227$. Both the VMI model and the CBS model are in excellent agreement with the experimental data.

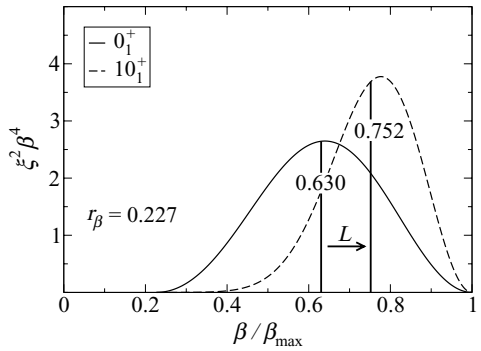

FIG. 8. Wave function densities of the 0_1^+ (solid line) and 10_1^+ (dashed line) states as a function of deformation, with the model parameter r_β set at 0.227. The centers of gravity of these distributions (vertical lines) are given in Table II as $\langle\beta/\beta_{max}\rangle(J)$.

with the experiment is quite satisfactory. Note that the CBS model is a fully quantum mechanical (albeit approximate) analytical solution of the Bohr-Hamiltonian, in contrast to the semiclassical VMI approach. We stress that this agreement between energy data and the CBS model is obtained by sole consideration of a soft potential in β that results in centrifugal stretching as a function of angular momentum. Figure 8 shows the wave function densities for the 0_1^+ ground state and the 10_1^+ state obtained from the CBS model as a function of the normalized deformation parameter β/β_{max}. With increasing angular momentum, the center of gravity of the CBS wave functions shifts to larger values of deformation $\langle\beta/\beta_{max}\rangle$. The second column of Table II lists the values of $\langle\beta/\beta_{max}\rangle$ from the CBS rotor model for the model parameter $r_\beta = \beta_{min}/\beta_{max} = 0.2269(8)$ obtained from a fit to the energies.

Next it is interesting to see whether the predicted increase of deformation with spin is reflected in our data on the $E2$ transition rates. For the sake of comparison we define the transitional quadrupole moments (Q_t values) from the model wave functions and from the $E2$ data in the usual fashion:

$$Q_t(J_i) = \frac{\sqrt{16\pi}}{\sqrt{5}\langle J_i K 20|J_f K\rangle}\sqrt{B(E2; J_i \to J_f = J_i - 2)}. \tag{15}$$

TABLE II. Average deformations of the CBS wave functions as a function of angular momentum are given in columns 2 and 3 of the table. They are in good agreement with the experimental deformation parameters in column 4, calculated by means of Eq. (16), which represents an off-diagonal matrix element. The absolute fluctuations of these deformations and their relative values (see text) are shown in the fifth and sixth columns.

J	$\langle\beta/\beta_{max}\rangle(J)$	$\langle\beta\rangle(J)$	$\langle\beta\rangle_{Expt.}(J)$	$\Delta\beta(J)$	$\Delta\beta/\langle\beta\rangle$
0_1^+	0.630	0.267	–	0.058	0.218
2_1^+	0.645	0.273	0.263(5)	0.057	0.209
4_1^+	0.673	0.285	0.278(7)	0.054	0.191
6_1^+	0.704	0.298	0.286(8)	0.051	0.170
8_1^+	0.730	0.309	0.309(19)	0.047	0.151
10_1^+	0.752	0.318	0.314(22)	0.043	0.137

The transitional quadrupole moment is connected with the average deformation of the nucleus via

$$Q_t(J_i) = \frac{3}{5\pi} Z\, e\, R^2\, \langle\beta\rangle_{Expt.}(J_i). \tag{16}$$

The $B(E2)$ values in the CBS rotor model are obtained with the $E2$ operator

$$\hat{T}(E2) = e_{eff}\,\hat{\beta} \tag{17}$$

in leading order. $Q_t(J)$ is constant in the rigid rotor limit. The values for $Q_t(J)$ as predicted by the VMI model are calculated by using the expression

$$Q_t(J) = k\sqrt{\frac{\mathcal{I}(J) + \mathcal{I}(J-2)}{2}}, \tag{18}$$

with the scale parameter k, fitted to data in Ref. [11]. To be independent of scales we consider the ratio

$$\frac{Q_t(J_1^+)}{Q_t(2_1^+)} \tag{19}$$

for the measured data, the rigid rotor, the VMI, and the CBS model. The results are plotted in Fig. 9. Both models, which account for an increasing moment of inertia with increasing spin, clearly agree with our new $E2$ data within the present experimental uncertainties. While the VMI model does not explain the origin of the spin dependence of $\mathcal{I}$, we observe that the CBS rotor model describes both the variable moment of inertia and the increase of $Q_t(J)$ as a function of spin in ^{168}Hf quantitatively in a purely geometrical way. The geometrical CBS model correctly predicts the increase of quadrupole deformation along the ground state band from a fit to the data on excitation energies that solely involves the concept of centrifugal stretching. The scale parameters $\beta_{max} = 0.423(7)$ and $\hbar^2/B = 7.62(26)$ keV were obtained from a fit to the ground state band excitation energies up to $E_x(10_1^+)$ and the four newly measured $B(E2; J \to J-2)$ transition rates. From Fig. 8 we conclude that the wave functions contain pieces with deformation ranging from $0.227\beta_{max} = 0.096$ to $\beta_{max} = 0.423$. Their fluctuations are quite substantial. The absolute fluctuations $\Delta\beta = \sqrt{\langle\beta^2\rangle - \langle\beta\rangle^2}$ and their relative

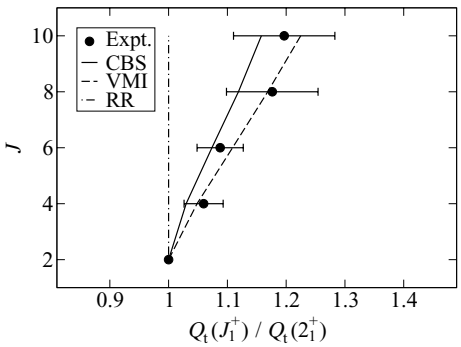

FIG. 9. Theoretical and experimental $Q_t(J_1^+)/Q_t(2_1^+)$ ratios as a function of spin, J, in ^{168}Hf. The vertical line represents the rigid rotor prediction while the dashed curve shows the VMI prediction as given in Ref. [11]. The solid curve represents the prediction of the CBS rotor model with the $E2$ operator in the lowest order as given in Eq. (17).

values $\Delta\beta/\langle\beta\rangle$ deduced from the wave functions of the CBS rotor model are shown in the fifth and sixth columns of Table II. The quantum fluctuations of the quadrupole deformation along the ground state band are substantial. They amount to about 20% of the mean deformation. This indicates that even a close to midshell nucleus in the $A \approx 170$ mass region like ^{168}Hf must be considered in terms of soft potentials as a function of deformation that allows for large quantum fluctuations. Modern geometrical models such as the analytical X(5) solution, the CBS rotor model, or the Davidson potential do this.

Shape invariants [18,19] give information about nuclear deformations and are therefore connected to the deformation parameters β and γ and their fluctuations. The quartic shape invariant K_4 [20] is related to fluctuations in the deformation variable β. Calculated for the CBS ground state wave function with structural parameter $r_\beta = 0.227$ it amounts to $K_4 = 1.174$. This value corresponds to a situation between the shape phase transitional point with $K_4 = 1.240$ for X5 and the rigid rotor limit $K_4 = 1$.

In summary, we measured lifetimes along the ground state band for the 4^+, 6^+, 8^+, and 10^+ states in ^{168}Hf. The results are consistent with the concept of centrifugal stretching and are fitted well by the CBS rotor model predictions with one parameter (r_β) that has been previously fixed from level energies.

ACKNOWLEDGMENTS

Help from the A. W. Wright NSL accelerator staff and from A. Lipski for providing excellent beams and technical support is gratefully acknowledged. We thank A. Dewald for useful discussions regarding the DDCM and I. Hamamoto for discussions. This work was supported by the US National Science Foundation under Grant PHY-0245018, by the US DOE under Grants DE-FG02-04ER41334 and DE-FG02-91ER40609, and by the Deutsche Forschungsgemeinschaft under Grant SFB 634.

[1] F. Iachello, Phys. Rev. Lett. **87**, 052502 (2001).
[2] R. F. Casten and N. V. Zamfir, Phys. Rev. Lett. **87**, 052503 (2001).
[3] R. Krücken *et al*., Phys. Rev. Lett. **88**, 232501 (2002).
[4] D. Tonev, A. Dewald, T. Klug, P. Petkov, J. Jolie, A. Fitzler, O. Möller, S. Heinze, P. von Brentano, and R. F. Casten, Phys. Rev. C **69**, 034334 (2004).
[5] A. Bohr, Mat. Fys. Medd. K. Dan. Vidensk. Selsk. **26**, No. 14 (1952).
[6] S. Devons, G. Manning, and D. St. P. Bunbury, Proc. Phys. Soc. A **68**, 18 (1955).
[7] A. Dewald, S. Harissopulos, and P. von Brentano, Z. Phys. A **334**, 163 (1989).
[8] G. Böhm, A. Dewald, P. Petkov, and P. von Brentano, Nucl. Instrum. Methods Phys. Res. A **329**, 248 (1993).
[9] N. Pietralla and O. M. Gorbachenko, Phys. Rev. C **70**, 011304(R) (2004).
[10] K. Dusling and N. Pietralla, Phys. Rev. C **72**, 011303(R) (2005).
[11] M. A. J. Mariscotti, G. Scharff-Goldhaber, and B. Buck, Phys. Rev. **178**, 1864 (1969).
[12] B. Bochev, S. Iliev, R. Kalpakchieva, S. A. Karamian, T. Kutsarova, E. Nadjakov, and Ts. Venkova, Nucl. Phys. **A282**, 159 (1977).
[13] E. A. McCutchan *et al*., Phys. Rev. C **76**, 064307 (2007).
[14] B. Saha, A. Dewald, O. Möller, R. Peusquens, K. Jessen, A. Fitzler, T. Klug, D. Tonev, P. von Brentano, J. Jolie, B. J. P. Gall, and P. Petkov, Phys. Rev. C **70**, 034313 (2004).
[15] O. Möller *et al*., Phys. Rev. C **74**, 024313 (2006).
[16] P. Petkov, D. Tonev, J. Gableske, A. Dewald, and P. von Brentano, Nucl. Instrum. Methods Phys. Res. A **437**, 274 (1999).
[17] V. S. Shirley, Nucl. Data Sheets **71**, 261 (1994).
[18] K. Kumar, Phys. Rev. Lett. **28**, 249 (1972).
[19] D. Cline, Annu. Rev. Nucl. Part. Sci. **36**, 683 (1986).
[20] V. Werner, N. Pietralla, P. von Brentano, R. F. Casten, and R. V. Jolos, Phys. Rev. C **61**, 021301(R) (2000).